Two-fluid Rayleigh-Marangoni-Bénard convection

K.A. Cliffe and S.J. Tavener

University of Nottingham and Colorado State University

Motivations

1.) Liquid encapsulated vertical Bridgeman crystal growth.

2.) Thermally as well as viscously and coupled flows when heated from below.

3.) Thermocapillary instability when heated from above.

4.) Loss of stability of the conducting solution to time-periodic flows.

Review articles

Johnson & Narayanan (1999) A tutorial on the Rayleigh-Marangoni-Bénard problem with multiple layers and side wall effects. *Chaos* **9**, pp. 124–140.

Andereck, Colovas, Degan & Renardy (1998) Instabilities in two layer Rayleigh-Bénard convection: overview and outlook. *Int. J. Engr. Sci.* **36**, pp. 1451–1470.

Experimental reference

Juel, Burgess, McCormick, Swift & Swinney (2000) Surface tension-driven convection patterns in two liquid layers. *Phyica D,* **143**, pp. 169–186.

Some earlier work

Renardy & Renardy (1985) Perturbation analysis of steady and oscillatory onset in a Bénard problem of two fluids. *Phys. Fluids* **28**, pp. 2699–.

Zeren & Reynolds (1985) Thermal instabilities in two-fluid horizontal layers. *J. Fluid Mech.* **53**, pp. 305–.

Two-fluid Rayleigh-Marangoni-Bénard convection.

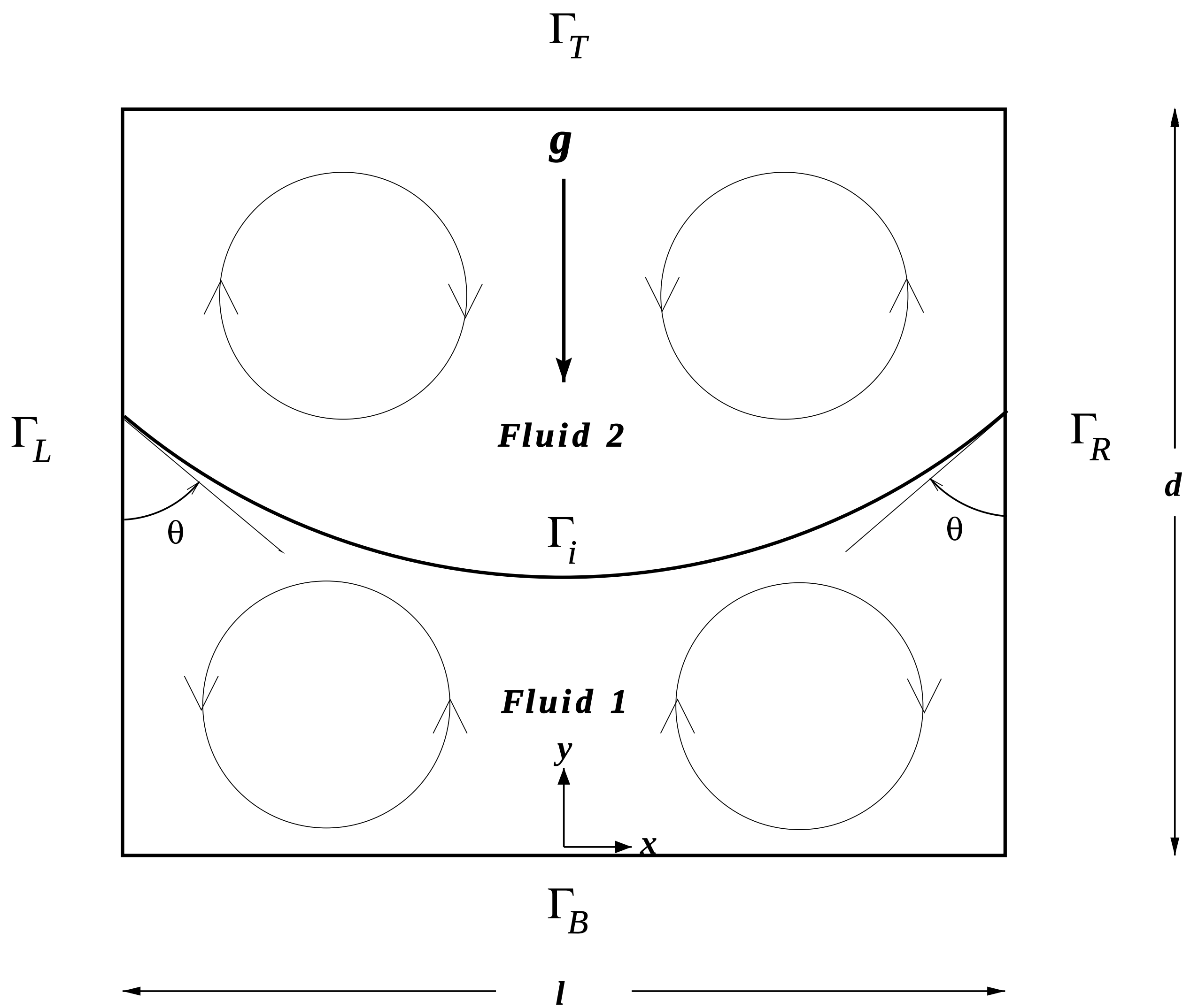

Applying the Boussinesq approximation, the system of equations governing two-fluid Rayleigh-Marangoni-Bénard convection in finite two-dimensional domains is

$$\begin{aligned}
\nabla_* \cdot \boldsymbol{u}^* &= 0, \\
\bar{\rho}_m \left(\frac{\partial u^*}{\partial t^*} + (\boldsymbol{u}^* \cdot \nabla_*)\boldsymbol{u}^* \right) &= \nabla_* \cdot \tau_m^* - \rho_m g \boldsymbol{j}, \\
\bar{\rho}_m c_m \left(\frac{\partial T^*}{\partial t^*} + (\boldsymbol{u}^* \cdot \nabla) T^* \right) &= \nabla_* \cdot (k_m \nabla_* T^*),
\end{aligned}$$

where $\rho_m = \bar{\rho}_m(1 - \alpha_m(T^* - \bar{T}^*))$ is the density of liquid m, c_m is the specific heat capacity, k_m is the thermal conductivity and

$$\tau_m^* = -p^* \boldsymbol{I} + \mu_m \left(\nabla_* \boldsymbol{u}^* + (\nabla_* \boldsymbol{u}^*)^T \right)$$

is the stress tensor, where μ_m is the molecular viscosity.

The subscript $m = 1, 2$ denotes the lower and upper fluids respectively, * denotes dimensional quantities and $\bar{T}^*$ is a fixed reference temperature.

The boundary conditions at the interface are

$$\begin{aligned} \boldsymbol{u}^* \cdot \boldsymbol{n} &= 0, \\ [\tau^* \cdot \boldsymbol{n}] &= -K^* \sigma\, \boldsymbol{n} - (\boldsymbol{t} \cdot \nabla \sigma)\, \boldsymbol{t}, \end{aligned}$$

where $[\cdot]$ denotes the jump across the interface.

Here K^* is the (dimensional) curvature of the interface, and $\boldsymbol{n}$ and $\boldsymbol{t}$ are the normal and tangential unit vectors respectively. (By convention, $\boldsymbol{n}$ is the normal pointing from fluid 1 into fluid 2.)

The interfacial tension is assumed to depend linearly on temperature, and

$$\sigma = \sigma_0 - \sigma_1 (T^* - \bar{T}^*).$$

The thermal flux is continuous across the interface.

The governing equations and boundary conditions were non-dimensionalized using

1.) length scale, $d = d_1 + d_2$,

2.) velocity scale, $\bar{U} = \dfrac{\kappa_1}{d}$,

where κ_1 is the thermal diffusivity of the lower fluid, $\kappa_1 = k_1/(\bar{\rho}_1 c_1)$. The corresponding time and stress scales are

3.) time scale $= \dfrac{d^2}{\kappa_1}$,

4.) stress scale $= \dfrac{\mu_1 \kappa_1}{d^2}$,

respectively.

The temperature was nondimensionalized according to

$$T = (T^* - \bar{T}^*)/\Delta T^*,$$

where ΔT^* is one-half the temperature difference between the top and bottom boundaries.

The corresponding non-dimensionalized weak forms of the steady momentum and temperature equations can be written as

$$\begin{aligned}
&\int_{\Omega_1} \Bigg[\left(\frac{1}{Pr} (\boldsymbol{u} \cdot \nabla) \boldsymbol{u} + \big(G - Ra\, T\big) \boldsymbol{j} \right) \cdot \boldsymbol{w} \\
&\qquad - p\, \nabla \cdot \boldsymbol{w} + (\nabla \boldsymbol{u} + \nabla \boldsymbol{u}^T) : \nabla \boldsymbol{w} \Bigg] \, \mathrm{d}A \\
+ \quad &\int_{\Omega_2} \Bigg[\rho_r \left(\frac{1}{Pr} (\boldsymbol{u} \cdot \nabla) \boldsymbol{u} + \big(G - \alpha_r Ra\, T\big) \boldsymbol{j} \right) \cdot \boldsymbol{w} \\
&\qquad - p\, \nabla \cdot \boldsymbol{w} + \mu_r (\nabla \boldsymbol{u} + \nabla \boldsymbol{u}^T) : \nabla \boldsymbol{w} \Bigg] \, \mathrm{d}A \\
+ \quad &\int_{\Gamma_i} \left[\left(\frac{1}{Ca} - Ma\, T \right) \boldsymbol{t} \cdot \frac{d\boldsymbol{w}}{ds} \right] \mathrm{d}s = 0,
\end{aligned}$$

and

$$\begin{aligned}
&\int_{\Omega_1} \Big[(\boldsymbol{u} \cdot \nabla) T S + \nabla T \cdot \nabla S \Big] \, \mathrm{d}A \\
+ \quad &\int_{\Omega_2} \Big[\rho_r c_r (\boldsymbol{u} \cdot \nabla) T S + k_r \nabla T \cdot \nabla S \Big] \, \mathrm{d}A = 0,
\end{aligned}$$

where Ω_1, Ω_2 are the two fluid regions, Γ_i is the interface between them, and $\boldsymbol{w}$ and S are test functions.

The nondimensional parameters are the Prandtl number Pr, Galileo number G, capillary number Ca defined by

$$Pr = \frac{\nu_1}{\kappa_1}\,, \quad G = \frac{gd^3}{\nu_1\kappa_1}\,, \quad Ca = \frac{\mu_1\kappa_1}{\sigma_0 d}\,,$$

and the Rayleigh number Ra and Marangoni number Ma defined by

$$Ra = \frac{g\alpha_1\Delta T^* d^3}{\nu_1\kappa_1}\,, \quad Ma = \frac{\sigma_1\Delta T^* d}{\mu_1\kappa_1}\,,$$

where $\nu_1 = \mu_1/\bar{\rho}_1$. The aspect ratio

$$\Gamma = \frac{l}{d}\,,$$

and the ratios $\rho_r, \alpha_r, \mu_r, c_r$ and k_r are

$$\rho_r = \frac{\bar{\rho}_2}{\bar{\rho}_1}\,,\ \alpha_r = \frac{\alpha_2}{\alpha_1}\,,\ \mu_r = \frac{\mu_2}{\mu_1}\,,\ c_r = \frac{c_2}{c_1}\,,\ k_r = \frac{k_2}{k_1}\,.$$

Continuity of thermal flux is assured by considering the integrals along the boundaries which arise upon integrating by parts.

To resolve the location of the interface these equations were coupled to a Landau coordinate transformation

$$
\begin{aligned}
x = A\phi,\ y &= 2h\psi && \text{in fluid 1,}\\
x = A\phi,\ y &= 1-2(1-h)(1-\psi) && \text{in fluid 2,}
\end{aligned}
$$

where A is a constant depending upon the aspect ratio of the domain, $h = h(\phi)$ is the (unknown) height of the interface and

$$
\begin{aligned}
(\phi,\psi) &\in ([0,1]\times[0,0.5]) \text{ for fluid 1,}\\
(\phi,\psi) &\in ([0,1]\times[0.5,1]) \text{ for fluid 2.}
\end{aligned}
$$

The (unknown) height of the interface $h = h(\psi)$ was then calculated by solving

$$\frac{\partial h}{\partial \phi} = 0\,,$$

which in weak form becomes

$$\int_{\Omega_1} \frac{\partial h}{\partial \phi}\,\zeta\;\mathrm{d}A + \int_{\Omega_2} \frac{\partial h}{\partial \phi}\,\zeta\;\mathrm{d}A = 0,$$

with test function ζ.

(We have previously used an orthogonal mapping technique.)

Boundary conditions, FEM and test computations

1.) Nonslip boundary conditions were imposed at horizontal and vertical solid boundaries.

2.) The temperature was specified along the top and bottom surfaces and adiabatic conditions were applied at the vertical walls.

3.) The relative volume fractions of the two fluids was specified as were the two contact angles.

The F.E.M. and test computations

1.) All computations were performed using the finite-element method employing quadrilateral elements with biquadratic interpolation of the velocity field, temperature field, mapping variable h and discontinuous linear interpolation of the pressure field.

2.) Numerical bifurcation techniques based on the construction and solution of extended systems were used to locate singularities. The reflectional symmetry about the vertical midplane was utilized when appropriate.

3.) Comparisons were made with previous calculations of Rayleigh-Marangoni-Bénard convection in a layer of a single fluid in the appropriate limit.

The role of symmetry

The nonlinear system of equations resulting from the finite-element discretization may be written as

$$\boldsymbol{f}(\boldsymbol{a},\boldsymbol{b}) = \boldsymbol{0}, \quad \boldsymbol{f} : \mathbf{R}^N \times \mathbf{R}^p \mapsto \mathbf{R}^N. \tag{1}$$

Let S be a finite-dimensional representation of the reflectional symmetry operator about $\psi = 0$, thus S is an $(N \times N)$ orthogonal matrix, where $S^2 = I$, but $S \neq I$. The finite-dimensional system of nonlinear algebraic equations (1) is equivariant with respect to S, i.e.

$$S\boldsymbol{f}(\boldsymbol{a},\boldsymbol{b}) = \boldsymbol{f}(S\boldsymbol{a},\boldsymbol{b}).$$

The orthogonal matrix S induces a unique decomposition of $\mathbf{R}^N$ into symmetric and antisymmetric subspaces,

$$\mathbf{R}^N = \mathbf{R}^N_s \oplus \mathbf{R}^N_a,$$

where

$$\begin{aligned}
\mathbf{R}^N_s &= \{\boldsymbol{x} \in \mathbf{R}^N : S\boldsymbol{a} = \boldsymbol{a}\}, \\
\mathbf{R}^N_a &= \{\boldsymbol{x} \in \mathbf{R}^N : S\boldsymbol{a} = -\boldsymbol{a}\}.
\end{aligned}$$

Symmetric solutions are those for which

$$
\begin{aligned}
h(\psi,\phi) &= h(-\psi,\phi), \\
u(\psi,\phi) &= -u(-\psi,\phi), \\
v(\psi,\phi) &= v(-\psi,\phi), \\
p(\psi,\phi) &= p(-\psi,\phi), \\
T(\psi,\phi) &= T(-\psi,\phi).
\end{aligned}
$$

Anti-symmetric solutions are those for which

$$
\begin{aligned}
h(\psi,\phi) &= -h(-\psi,\phi), \\
u(\psi,\phi) &= u(-\psi,\phi), \\
v(\psi,\phi) &= -v(-\psi,\phi), \\
p(\psi,\phi) &= -p(-\psi,\phi), \\
T(\psi,\phi) &= -T(-\psi,\phi).
\end{aligned}
$$

Symmetry-breaking bifurcation

At a symmetry-breaking bifurcation point $(\boldsymbol{a}_0, \boldsymbol{b}_0)$,

$$\left.\frac{\partial \boldsymbol{f}}{\partial \boldsymbol{a}}\right|_{(\boldsymbol{a}_0, \boldsymbol{b}_0)} \boldsymbol{z} = \boldsymbol{0},$$

where $\boldsymbol{a}_0 \in \mathbf{R}_s^N$ and the null eigenvector, $\boldsymbol{z} \in \mathbf{R}_a^N$. Since the symmetries of the solution and eigenvector are known, all computations may be performed in one-half of the domain. Symmetry breaking occurs generically at a pitchfork bifurcation point.

Subspace-breaking bifurcation

For 90 degree contact angles, the conducting solution exists for all Marangoni numbers. Subspace breaking occurs generically at a transcritical bifurcation point. For contact angles other than 90 degrees, this conducting solution (subspace) does not exist.

Fluid properties of acetonitrile and n-hexane as reported by Juel *et al* (2000).

Property	acetonitrile	n-hexane
ρ (10^3 kg m^{-3})	0.776	0.655
ν (10^{-6} m^2 s^{-1})	0.476	0.458
k (10^{-1} J m^{-1} s^{-1} K^{-1})	1.88	1.20
c_p (10^3 J kg^{-1} K^{-1})	2.23	2.27
α (10^{-3} K^{-1})	1.41	1.41
σ_0 (10^{-3} N m^{-1})	28.66	17.89
σ_1 (10^{-5} N m^{-1} K^{-1})	12.63	10.22

For this pair of fluids,

$$
\begin{aligned}
Ra &= 2.67 \times 10^{11}\, d^3\, \Delta T^*, \\
Ma &= 3.15 \times 10^{6}\, d\, \Delta T^*.
\end{aligned}
$$

Instability mechanism on heating from above

(e.g. Liquid encapsulated vertical Bridgeman growth)

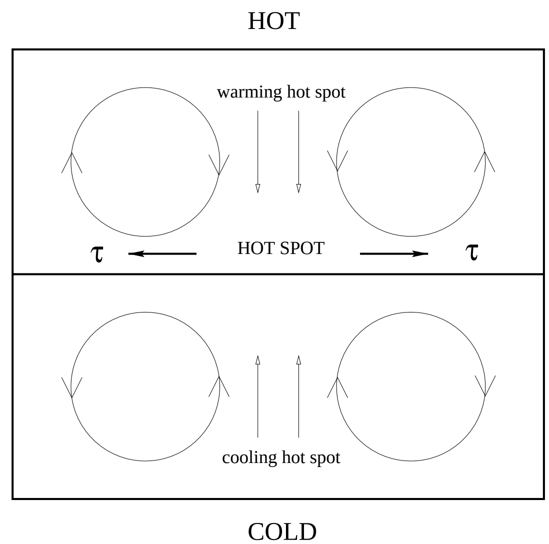

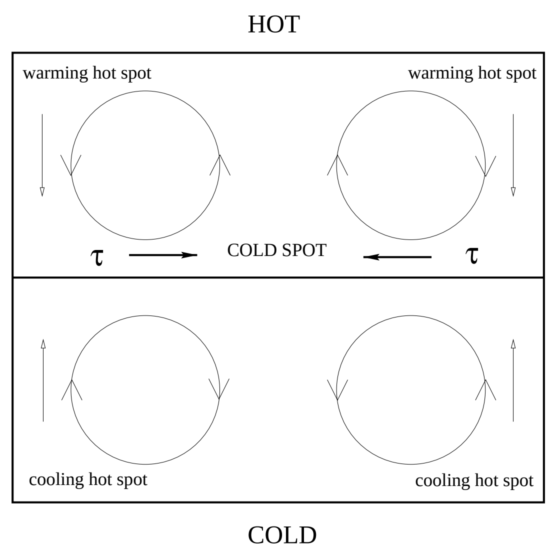

Bifurcation diagrams for aspect ratio $\Gamma = 1.5$

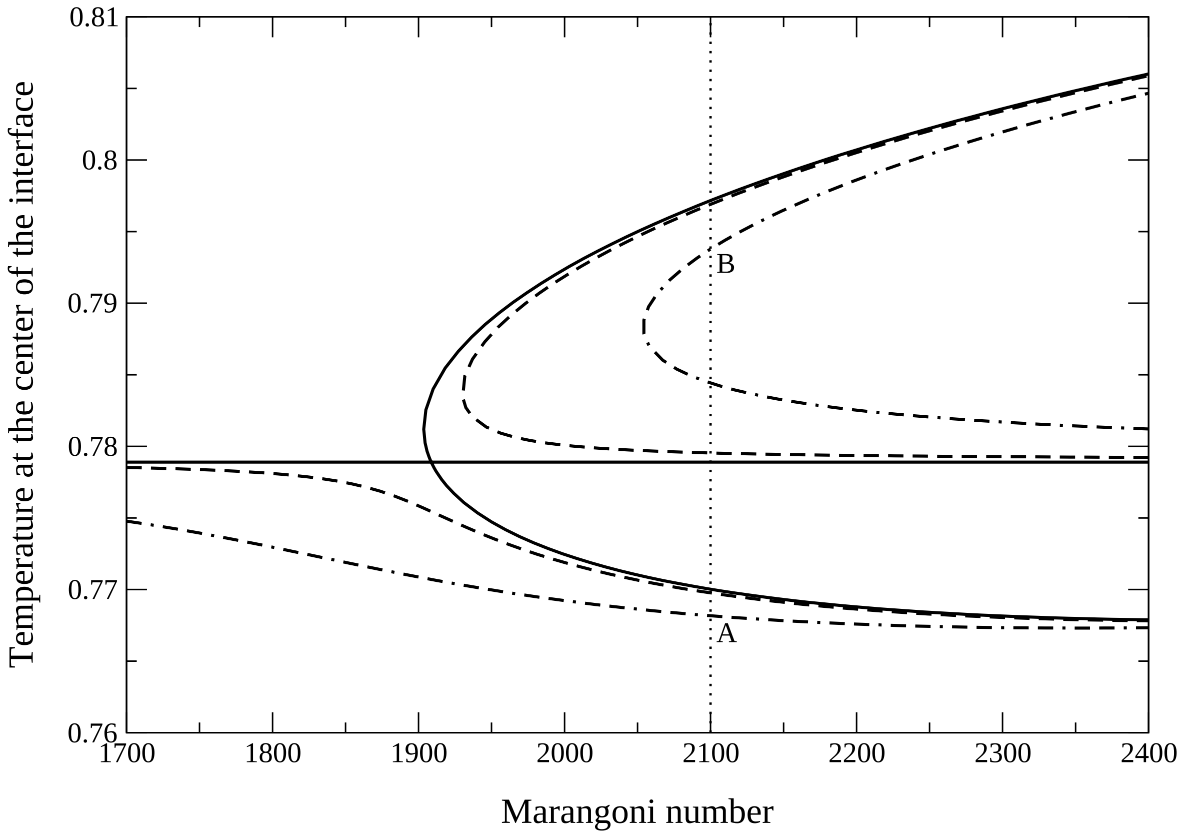

Contact angles equal to 90 (solid line), 89.99 (dashed line) and 89.89 (chained line) degrees. $Pr = 4.38,\ Ca = 2.5 \times 10^{-6},\ Ra = 0,\ G = 0,\ \rho_r = 0.844,\ \mu_r = 0.812,\ \alpha_r = 1.0,\ c_r = 1.02,\ k_r = 0.638,\ v_r = 1.0.$

Streamlines and isotherms at A and B

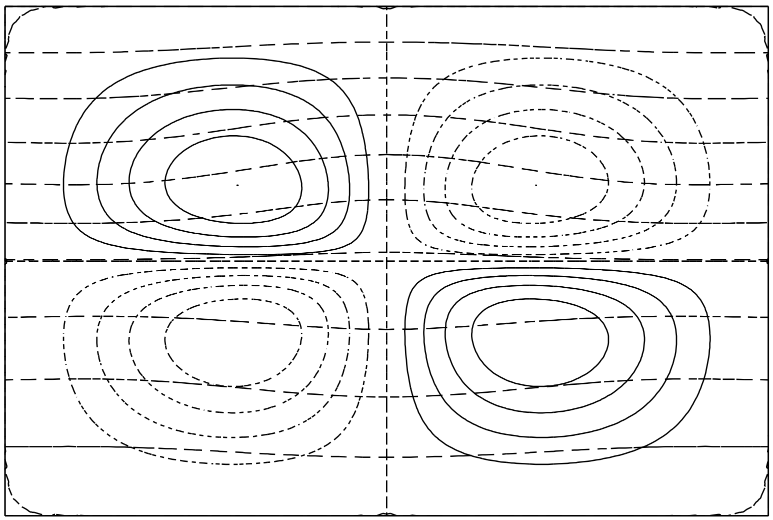

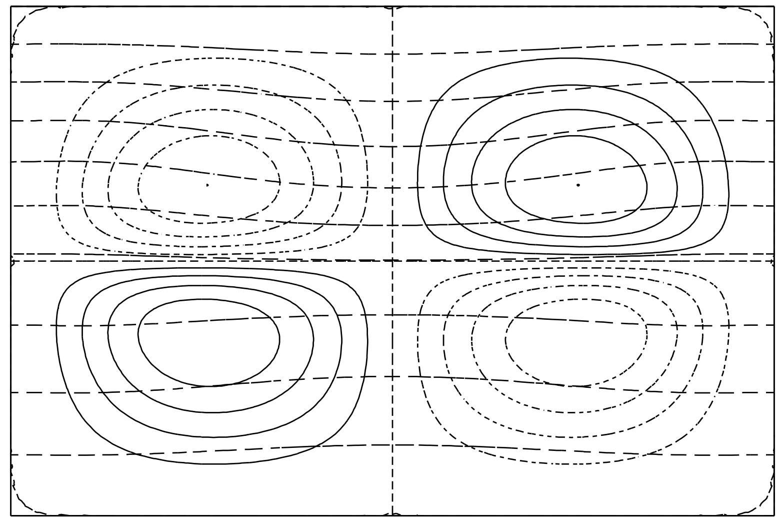

Investigation of parameter space at zero gravity

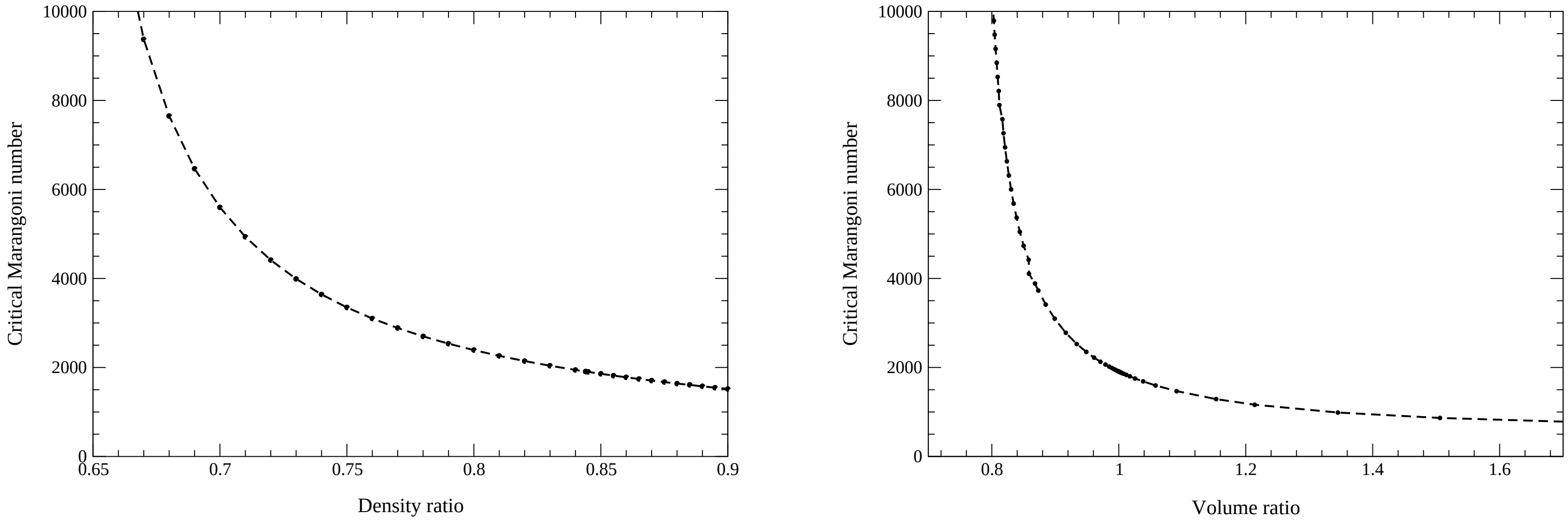

The effect of gravity (Buoyancy dominates as overall depth increases.)

The dashed line has slope 1. Since $Ma/Ra = (3.15 \times 10^6)/(2.67 \times 10^{11}\, d^2)$, the dotted lines which have slopes 1.5 and 5, correspond to depths 3cm and 1.5cm respectively in the experiments of Juel et al.

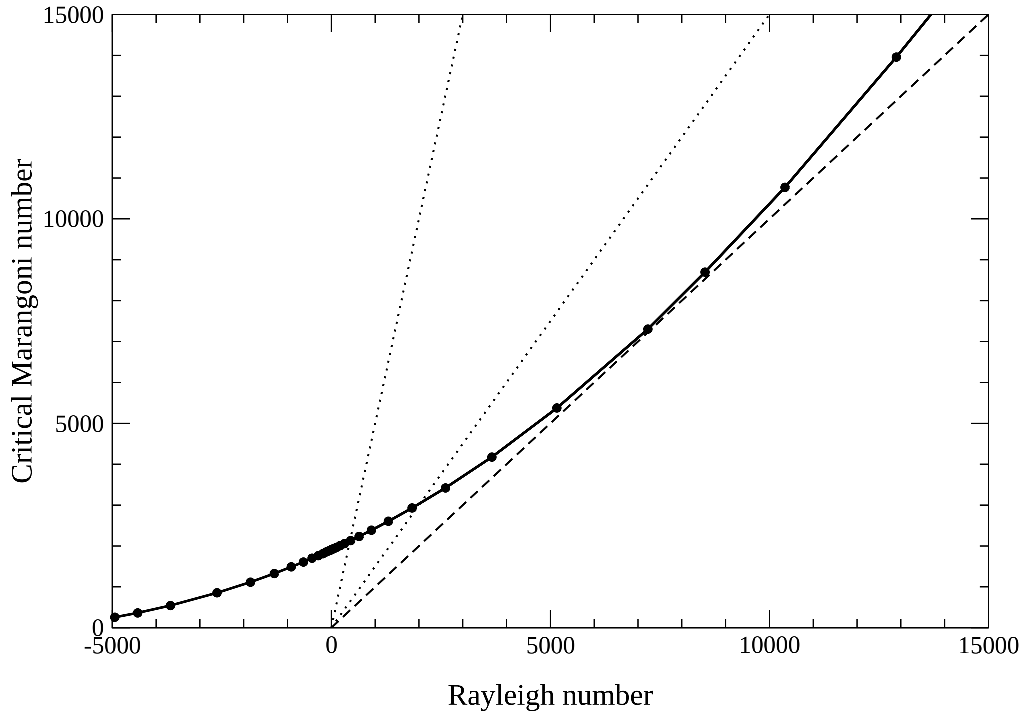

$Pr = 4.38,\ Ca = 2.5 \times 10^{-6}, G = 5, \times 10^4,\ \rho_r = 0.844,\ \mu_r = 0.812,\ \alpha_r = 1.0,\ c_r = 1.02,\ k_r = 0.638,\ v_r = 1.0,\ \Gamma = 1.5.$

Buoyancy vs. thermocapillarity

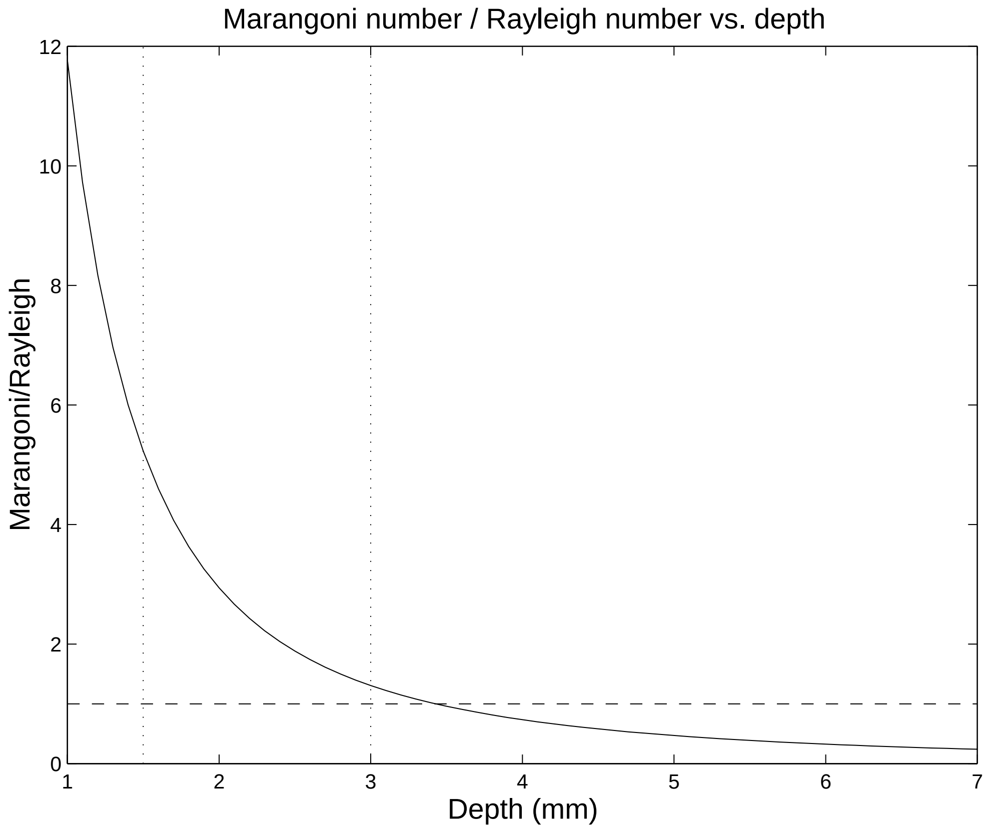

Thermocapillarity dominates

Buoyancy dominates

At overall depths of 1.5mm and 3mm the critical Marangoni number corresponds to a critical temperature differences across the cell of 0.4 and 0.3 degrees respectively, in good agreement with those reported by Juel et al (2000).

Future directions

1. Examine other experimental realizations of Juel *et al* (2000), especially those resulting in oscillatory convection.
2. Consider domains of more direct interest to the crystal growth industry, e.g. axisymmetric domains, including solid-liquid interfaces.
3. Investigate the effect of limited miscibility using a phase field approach - grid refinement!!.